View metadata, citation and similar papers at core.ac.uk

brought to you by CORE

provided by Elsevier - Publisher Connector

Cryo-electron microscopy reveals ordered domains in the immature HIV-1 particle

Stephen D. Fuller*, Thomas Wilk*, Brent E. Gowen*, Hans-Georg Kräusslich† and Volker M. Vogt‡

Background: Human immunodeficiency virus type1 (HIV-1) is the causative agent of AIDS and the subject of intense study. The immature HIV-1 particle is traditionally described as having a well ordered, icosahedral structure made up of uncleaved Gag protein surrounded by a lipid bilayer containing envelope proteins. Expression of the Gag protein in eukaryotic cells leads to the budding of membranous virus-like particles (VLPs).

Results: We have used cryo-electron microscopy of VLPs from insect cells and lightly fixed, immature HIV-1 particles from human lymphocytes to determine their organization. Both types of particle were heterogeneous in size, varying in diameter from 1200–2600 Å. Larger particles appeared to be broken into semi-spherical sectors, each having a radius of curvature of approximately 750 Å. No evidence of icosahedral symmetry was found, but local order was evidenced by small arrays of Gag protein that formed facets within the curved sectors. A consistent 270 Å radial density was seen, which included a 70 Å wide low density feature corresponding to the carboxy-terminal portion of the membrane attached matrix protein and the amino-terminal portion of the capsid protein.

Conclusions: Immature HIV-1 particles and VLPs both have a multi-sector structure characterized, not by an icosahedral organization, but by local order in which the structures of the matrix and capsid regions of Gag change upon cleavage. We propose a model in which lateral interactions between Gag protein molecules yields arrays that are organized into sectors for budding by RNA.

Addresses: *The Structural Biology Programme, European Molecular Biology Laboratory, Postfach 10.2209, Meyerhofstrasse 1, D-69012 Heidelberg, Germany. †Heinrich-Pette-Institut, Stiftung des Privaten Rechts, Martingasse 52, D-20251 Hamburg, Germany. ‡Section of Biochemistry, Molecular and Cell Biology, Biotechnology Building, Cornell University, Ithaca, New York, NY 14853, USA.

Correspondence: Stephen D. Fuller
E-mail: fuller@EMBL-Heidelberg.DE

Received: **10 June 1997**
Revised: **24 July 1997**
Accepted: **24 July 1997**

Published: **1 September 1997**

Current Biology 1997, 7:729–738
http://biomednet.com/elecref/0960982200700729

© Current Biology Ltd ISSN 0960-9822

Background

Retroviruses provide a strikingly simple example of enveloped virus assembly. A single protein, the product of the *gag* gene, is sufficient to carry out assembly and budding of virus-like particles (VLPs). The Gag molecule must make a number of specific interactions: with the plasma membrane; with the viral genomic RNA; with other Gag molecules; and with viral envelope protein molecules, separately transported to the plasma membrane by the cellular secretory pathway [1]. In the case of human immunodeficiency virus type 1 (HIV-1), like other retroviruses, the Gag protein is organized into domains corresponding to several distinct proteins of the mature virus: the membrane-associated or matrix protein (MA), the capsid protein (CA), and the nucleocapsid protein (NC). Gag also has one or more other domains with functions that are poorly understood (nomenclature reviewed in [2]). MA is myristylated and forms the amino-terminal domain of Gag. CA is believed to form the shell of the mature viral core. NC is highly basic and interacts directly with the RNA. Cleavage of the precursor Gag into domains by the viral protease leads to dramatic morphological changes called maturation [3,4].

The structures of HIV-1 particles, as well as those of other retrovirus particles, have been studied extensively, but a complete understanding of their organization remains elusive. Thin section electron microscopy (EM) shows a resemblance between the nascent, immature HIV-1 particle in the last stages of budding and the type C retrovirus budding particles of the prototypic murine leukemia viruses (MLVs) and avian sarcoma and leukemia viruses (ASLVs). Directly inside the membrane is an electron dense ring, that encloses an electron lucent center. In the virus mutants with a defective or inactivated protease, budding releases permanently immature particles into the medium [5,6]. In presence of a functional protease, maturation occurs, leading to the formation of an electron dense core in the middle of the virus particle. In HIV-1, this core takes the form of a cone, unlike the centrally located, spherical cores of type C viruses. The structures of mature retroviruses have remained particularly difficult to decipher by EM, because of the need to remove the membrane by detergents to visualize the internal structures. Immature cores appear stable to detergents, at least in crude sedimentation assays and thin section EM [7], but their detailed organization has not been elucidated.

Figure 1

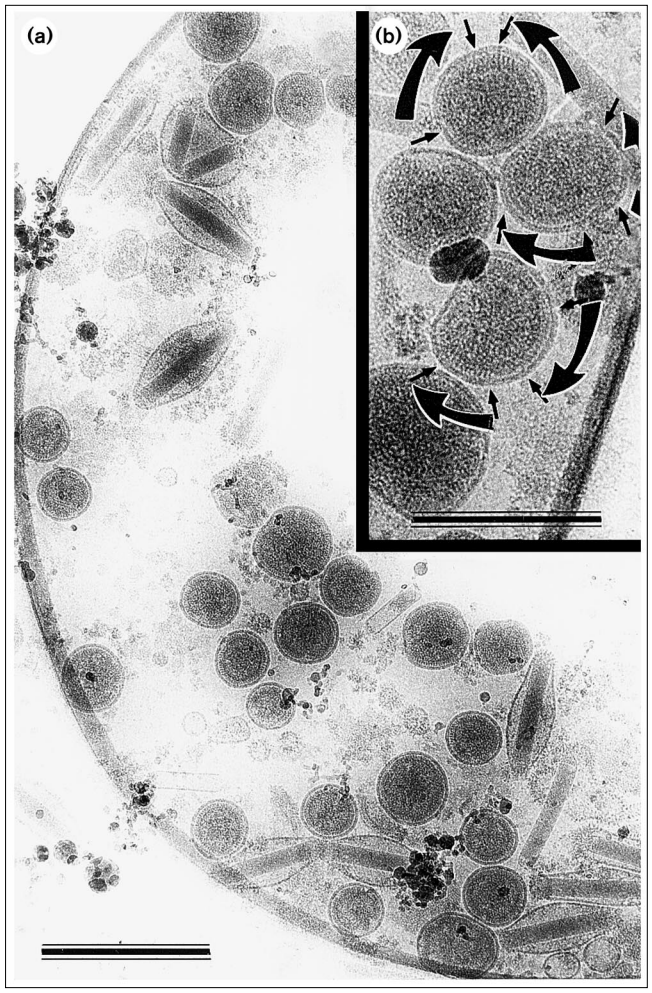

Cryo-electron micrographs of a field of Gag particles (VLPs), harvested rapidly after expression in insect cells, reveal their overall organization. **(a)** An overview in which both the round Gag particles and the elongated baculovirus particles are present. The internal structures within the membrane of the baculovirus virions are visible, as are the features extending from the membrane. The Gag particles show irregularities in shape and faults at the positions of these irregularities. Scale bar = 0.5 μm. **(b)** A detail revealing the rod-like Gag proteins perpendicular to the membrane and the faults (arrows) that occur at the boundaries of hemispherical sectors (arcs). Scale bar = 0.25 μm.

It has generally been accepted that both the immature and the mature retrovirus core are organized with icosahedral symmetry. This notion is partially based on analogy with the many other kinds of viruses that have been studied in detail by crystallography and by cryo-electron microscopy (cEM), and in part on limited experimental data. Early observations of HIV-1 particles reveal a pattern of surface antigen (SU) that could be indexed as a T = 7l icosahedral network [3]. Freeze-fracture work on the forming particle reveal that immature HIV-1 particles contain hexagonally arrayed Gag proteins, whose arrangement was interpreted as having T = 63 icosahedral symmetry [8]. Some evidence for icosahedral symmetry of MLV was presented many years ago [9], although a helical structure for the internal organization of this virus has also been suggested [10,11]. More recent work has based structural models on the assumption of icosahedral symmetry [8,12,13].

Membranous VLPs are readily obtained from insect cells infected with recombinant baculoviruses expressing the HIV-1 Gag protein. These VLPs have the advantage that they are abundant and non-infectious. VLPs closely resemble immature virions from protease-defective HIV-1 [14,15]. Thin section EM showed that VLPs appear as lipid-bound structures with a densely staining region ~180 Å in thickness [5,8,16–19] underneath the membrane and radial striations similar to those observed in immature HIV-1.

We have used cEM to study the structure of HIV-1 VLPs. This technique avoids fixatives, dehydration and contrasting agents, which are known to be destructive to the organization of membranous assemblies. Defocus phase contrast allows the visualization of these unstained structures and reveals the entire particle in projection. This allowed us to examine its symmetry as a whole, rather than inferring an organization from a portion of its surface. We describe the organization of the VLP and show that it is similar to that of the immature HIV-1 particle.

Results

Gag expression results in the budding of regular particles

HIV-1 VLPs were produced by expression in insect cells of the Gag protein, using a previously described baculovirus vector [14,15]. Stained SDS-polyacrylamide gels showed that the Gag protein was the single most abundant polypeptide in the preparation (not shown). All of our VLP preparations also contained baculovirus particles, as these have similar sedimentation properties. Preparations were examined by cEM within a few hours of purification. This rapid method of preparation was designed to preserve the structure of the particles rather than to enhance their biochemical homogeneity. Preparations isolated in the same way from cells that were infected with control baculovirus vectors (not shown) lacked the structures attributed to the VLPs below.

Typical samples of particles showed the characteristically rounded VLPs, elongated baculoviruses and cell debris (Figure 1a). The preservation of the baculovirus demonstrates the advantages of unstained microscopy for membrane structures. Most baculovirus virions remained intact and undistorted by the preparation for cEM. The baculovirus core could be readily visualized within the membrane, and envelope proteins were visible at the ends of the particle. The VLPs showed few surface features but a wealth of internal detail. Higher magnification (Figure 1b)

Figure 2

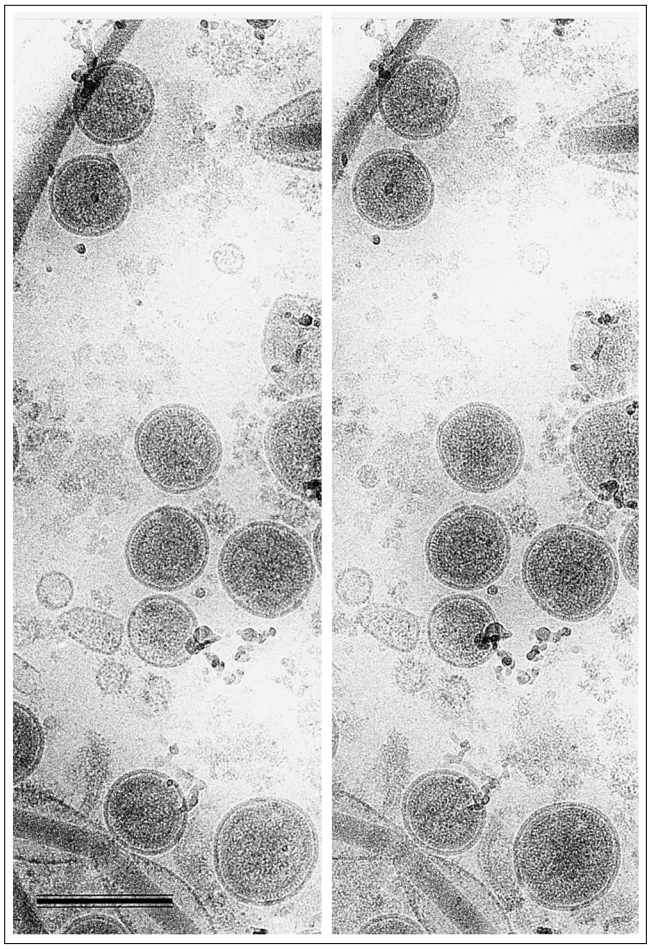

Stereo view of rapidly prepared Gag particles. The hemispherical sectors and irregularities at domain boundaries (faults) are visible. The faceted appearance of the particles is particularly clear in the particles in the center of the field. Note that the particles are within the body of the vitrified water layer rather than at the surfaces. Scale bar 0.25 μm.

revealed rod-like features underneath the membrane, 150–200 Å in projected length, with a center-to-center distance of ~55 Å. The VLPs displayed variability in size and shape. Particles that appeared intact ranged in diameter from 1200–2600 Å (mean ~1600 Å, mode ~1400 Å). Smaller particles were also present, but they appeared largely empty, lacked the organized rod like features described above and could be found in the baculovirus controls.

The VLPs that were visualized shortly after harvesting do not have a smooth, circular appearance. Instead, they often appeared to comprise two or more semi-spherical sectors. These sectors are marked with arcs in Figure 1 and have a characteristic radius of curvature of slightly over 750 Å. The sectors were most evident in larger particles. The boundary between two sectors in a particle was typically marked by an interruption in the regular density that lay under the membrane. Several instances of these faults — positions in which the close packing of the Gag rods is interrupted — are marked by arrows in Figure 1b.

The semi-spherical nature of the sectors was most easily visualized in stereo images of rapidly harvested VLPs (Figure 2). Regions of lower density can be seen at the boundaries of these domains. The stereo image also reveals that the sub-membrane arrays of Gag protein form flattened surfaces or facets within the particles. The facets reflect the intrinsic geometry of the particles, rather than interaction with the air–water interface during vitrification, as it is apparent from the stereo images that the VLPs tend to occupy the middle of the ~2000 Å thick water layer.

As the VLPs are not truly spherical, it would be misleading to assign them a unique diameter. Nevertheless, systematic analysis of the particle dimensions is revealing. Figure 3 indicates the maximum and minimum diameters that we used to describe these non-spherical structures, for which an average diameter can be calculated from a

Figure 3

Quantitative analysis of Gag particle dimensions. **(a)** The average width is the average of several measurements across the particle, including those which are not diameters, and is shown for 142 VLPs in a rapidly harvested HIV-1 Gag preparation. Note that, while the modal width is between 1400–1600 Å, many larger particles exist in the preparation. The insert shows the definitions of maximum and minimum diameter used for evaluating the particles. **(b)** Larger particles are more aspherical – the departure of the ratio of the minimum to the maximum diameter from 1.0 is greater at larger average particle width. The dashed line shows the ratio of diameters for a spherical particle, while the solid line shows a linear regression line for the entire population.

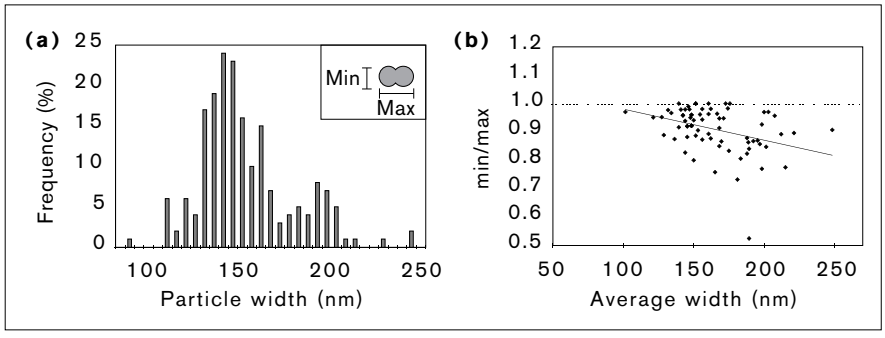

Figure 4

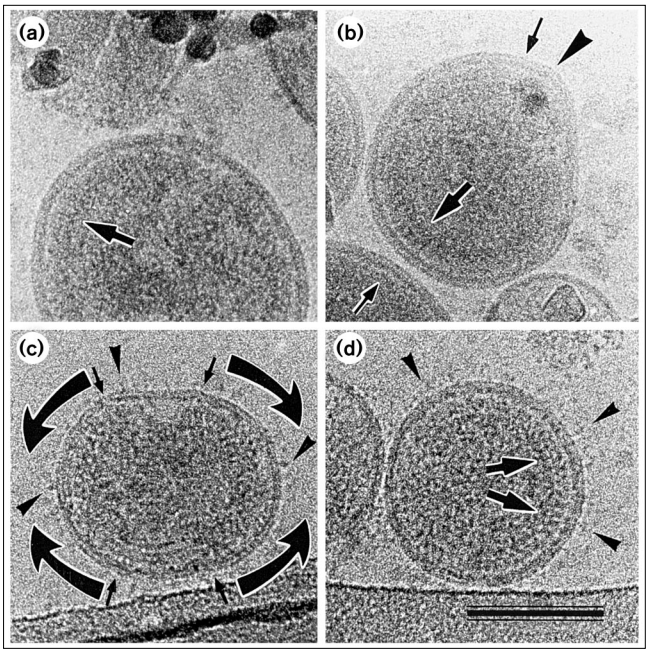

Comparison of VLPs and immature HIV-1. Cryo-electron micrographs of (a,b) Gag protein particles and (c,d) immature HIV-1 show their similar organization. The interaction between the rods of Gag protein beneath the membrane and density modulation within the membrane is revealed by the correspondence between positions of features in the two. **(a)** This micrograph shows the modulation of membrane density that matches the positions of the Gag protein rods (large arrow), which are packed side to side beneath the membrane. **(b)** This micrograph reveals the same membrane features in a distorted VLP when the sub-membrane rods are viewed perpendicular (large arrow) or at an angle to the direction of view (small arrow). Note that the modulation of density within the membrane is not seen in the region of the large fault (arrowhead) where the rods do not approach the membrane. The features of fixed, immature HIV-1 particles are seen in **(c)** and **(d)**. The rod-like Gag density, hemispherical sectors (arcs) and faults (arrows) that characterize the VLPs formed by Gag expression are visible in these immature HIV-1 particles. The presence of occasional SU domains on the HIV-1 particle surface (arrowheads) is, of course, unique to the HIV-1 particles. (Scale bar = 0.1 μm.)

series of measurements. The distribution of the ratios of the minimum to the maximum radius of the particles shows that larger VLPs are increasingly less spherical. The distribution of minimum diameters for the VLPs shows that the larger and smaller particles share a characteristic radius of slightly more than 750 Å (mean minimum diameter 1527 Å). The quantitative analysis supports a description of VLPs as accretions of semi-spherical sectors with a characteristic size.

This domain structure of the VLPs was labile. Particles that were harvested rapidly and vitrified immediately after harvest, such as those in Figures 1 and 2, showed the sectors most clearly. Particles that were harvested less rapidly, or held on ice overnight before vitrification, did not show these features so clearly. Instead, the particles appeared rounded and circular, and the faults that could still be observed were less obviously the boundaries of sectors. One could easily define a single diameter for each such particle and the population showed no well-defined minimum radius. This situation would match the dashed line in Figure 3b. Similar effects have been observed in other enveloped viruses, in which the particle becomes more rounded upon storage and looses its polyhedral shape [20].

The formation of VLPs requires the Gag protein, but not authentic genomic RNA. Most workers, however, have assumed that retrovirus VLPs incorporate cellular RNA, a supposition supported by *in vitro* assembly studies [21,22]. To support our contention (see below) that RNA is essential for particle assembly, we performed immunogold staining of sections of freeze-substituted VLPs with an anti-RNA antibody [23–25] and confirmed the presence of nucleic acid in VLPs of all size classes (not shown).

VLPs are not icosahedral

The observation that the VLPs are multi-domain structures that adopt a variety of sizes would seem to rule out any possibility that they are icosahedral. However, other enveloped viruses such as hepatitis B form both large and small capsids, which differ in triangulation number [26–29]. The variation in VLP size could reflect a similar variation. Accordingly, we selected a set of apparently undistorted particles of 1400 Å diameter and tested them for icosahedral symmetry using the well established common lines techniques [20,30–32].

The VLP data failed at all stages of this procedure. Orientations could be defined for individual particles, but their residuals were not significantly lower than the average of all possible orientations. Refinement of the position of the center of symmetry led to its movement away from the apparent center of the particle. Combining projections from different particles of similar size in the best orientations produced high interparticle residuals and did not produce consistent reconstructions. These problems do not result from lack of contrast at the resolution ranges studied, as VLP images contain more contrast between 500–700 Å radii (see below) than seen in images of alphaviruses, for which orientations can be determined easily [20,33–35]. Such a negative result is always equivocal, but analysis of the sub-membrane features of the VLPs using methods established for other membrane viruses yielded no evidence for their icosahedral nature.

Membrane interaction

Cryo-electron micrographs provided evidence for an interaction between the sub-membrane features and the membrane itself. Figure 4a shows a regular variation in contrast within the membrane that matches the spacing of

Figure 5

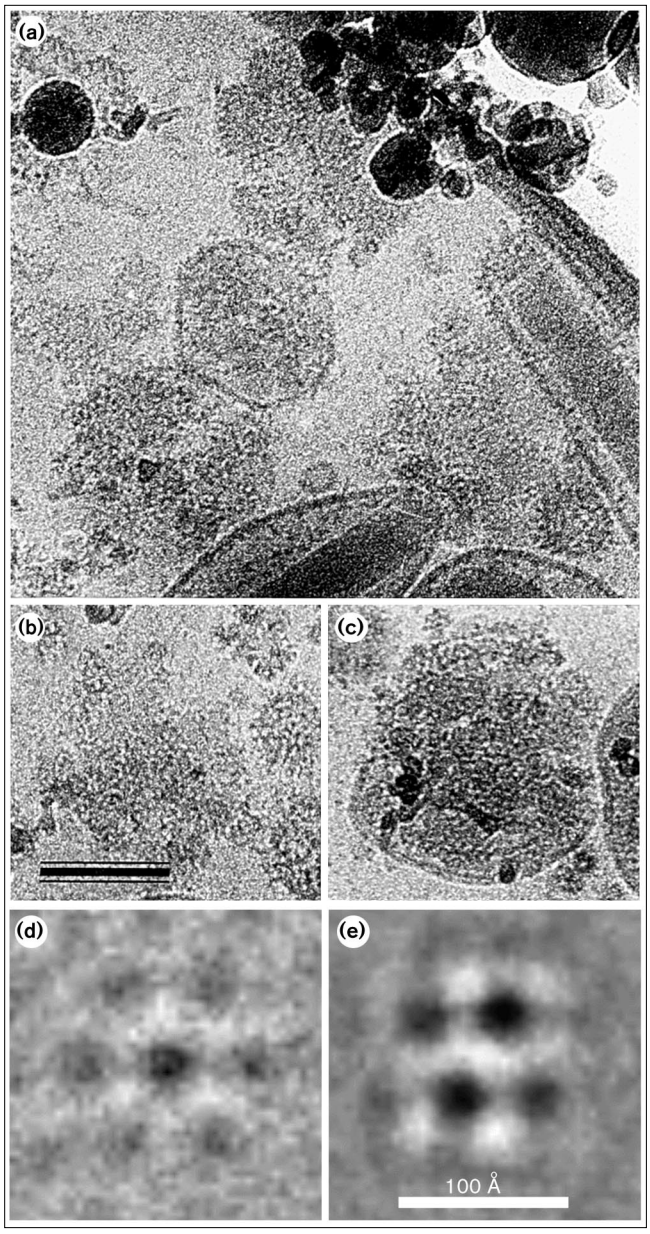

(a,b) The occurrence of small crystalline patches in a preparation of dissociated Gag particles. **(c)** A similar crystal on the surface of a dissociating Gag particle, indicating the correspondence between the facets of the particle surface and the crystalline patches. Correlation averages of Gag crystals were performed using a six-fold motif, a three-fold motif and an orthogonal motif. Each average was produced by aligning 4000 units using the motif to produce an intermediate average that was symmetrized and used to re-align the units and produce the average displayed. FRC [38] of two 2000 particle subaverages showed that alignment with the six-fold averaged motif produced an average **(d)** with a resolution worse than 50 Å. Further iterations of the averaging process converged toward the orthogonal result. The orthogonal average **(e)** of 4000 units produced in the same way had a resolution of 17 Å by the FRC criterion. A three-fold motif extracted from (e) produced a similar average, with 17 Å resolution, by the FRC criterion (not shown). Protein is dark in (a,b,c) and light in (d,e). (Scale bar = 0.1 μm.)

the sub-membrane density. The interruption of the sub-membrane density near a fault (arrowhead) is matched by a loss of the density modulation within the membrane. Images such as Figure 4b show that the interaction causes changes in curvature in the envelope and gives rise to the facets seen in the stereo images of Figure 2.

Several authors have suggested that the HIV-1 VLP should be a good model for the structure of the authentic immature HIV-1 particle, although the VLP lacks the other viral proteins, including Gag–Pol [5,8,16]. Nevertheless, we wished to be sure that the organization we observed in our VLPs, and in particular the variation in size and lack of icosahedral order, did not reflect the absence of these proteins or of the authentic full-length HIV-1 genome. Accordingly we used cEM to examine paraformaldehyde-inactivated HIV-1 particles produced by infection of MT4 cells [36] with an infectious proviral clone, pNL4-3.

Figures 4c and 4d show that these immature HIV-1 particles exhibit the same ordering of rod-like Gag protein, semi-spherical sectors (arcs) and faults (arrows) as seen in our VLP preparations. The immature HIV-1 particles also show occasional surface features corresponding to the SU protein, which are lacking in the VLP preparation as only the Gag protein is expressed by our baculovirus construct. The correspondence between paraformaldehyde-inactivated HIV-1 particles and the unfixed VLPs suggests that the organizational features that we describe here reflect properties of the authentic immature HIV-1.

Two-dimensional order

Although the VLPs as a whole do not display icosahedral order, the sub-membrane density does form small domains of two-dimensional crystallinity. This crystallinity is seen most easily when the particles are disrupted, so that the effects of superposition are minimized. Figure 5a shows dissociated particles that have released small crystalline areas of Gag. Examination of isolated arrays show that they are highly mosaic, but appear to show a monoclinic (p2) [37] organization (Figure 5b). An image of a partially disrupted virion (Figure 5c) shows regions of its surface contain arrays with the p2 organization seen in the isolated areas.

The small size of individual crystals meant that correlation methods were needed to average subunits and obtain a higher signal-to-noise ratio in the average. Accordingly, small regions were used as motifs for cross-correlation and rotational and translational alignment before averaging. Once such an average had been generated, it was used again in cross-correlation to produce a new average with higher signal-to-noise ratio. Averaging produced the asymmetric unit shown in Figure 5e, which was shown to be reliable to 17 Å by Fourier ring correlation (FRC) of independent averages [38].

Figure 6

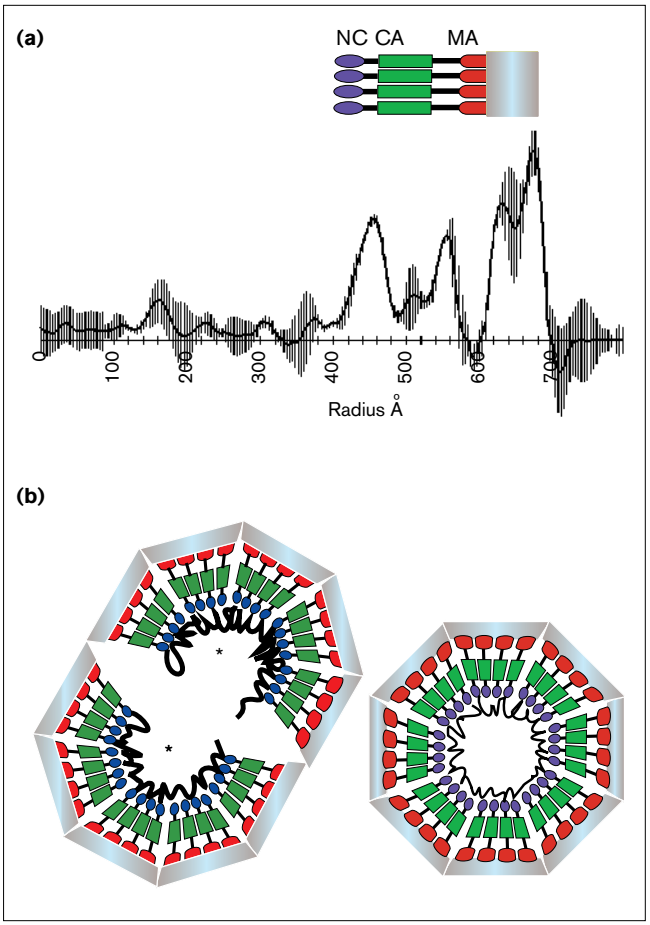

A model for HIV-1 structure and assembly. The average of eight Gag particle profiles, with the standard deviation shown as vertical lines, is shown in **(a)**. The horizontal axis shows distance in Å from the particle center at the left. A model for the radial placement of the Gag protein domains is presented as an interpretation of the profile. The individual components of the Gag protein are aligned with features in the radial density profile. The thickness of the isolated MA protein determined by X-ray crystallography and NMR is larger than the density next to the inner leaflet of the bilayer to which it corresponds in this profile. This suggests a conformational change at the CA–MA boundary occurs upon its cleavage during particle maturation. The schematic cross sections of two HIV-1 Gag particles in **(b)** show the presence of hemispherical sectors and the occurrence of faults at domain boundaries. The shading of the Gag protein is as in (a). Note that different segments of RNA will nucleate domains with different centers and give rise to the observed multi-domain structure.

The repeating unit comprises a dimer of three-fold structures. Correlation averaging with half of this unit, to which three-fold averaging had been applied, returned the three-fold unit with the same 17 Å resolution. Although the entire unit was clearly monoclinic (p2) [37], the unit cell angles in the plane were near to those expected for a hexagonal array. The expectation that a viral capsid should have local six-fold symmetry led us to repeat the correlation analysis with a six-fold averaged motif. This attempt produced degradation of the average (FRC analysis showed a resolution of 50 Å) and repeated rounds of averaging resulted in convergence to the p2 result.

Treatment of VLPs with the non-ionic detergent octyl glucoside removed the lipid bilayer, splitting the particle at its faults while leaving much of the local organization intact (not shown). This gives an indication of the hierarchy of interactions in the particle. The local interactions between Gag subunits persist in the absence of an intact membrane, although the global organization into sectors is destroyed.

Radial organization of the VLP

The variation in VLP diameter makes it difficult to define a radial density distribution in three dimensions. Indeed the simple averaging of the projected radial density for particles of different radii would lead to a blurring of features. A Fourier–Bessel method [39] was used to overcome this problem by averaging the three-dimensional radial density distributions from different radii of the particle after aligning them on the position of the membrane. Aligning these three-dimensional profiles of particles on the positions of low density corresponding to the bilayer allows calculation of an average profile. The average of eight particle profiles with their standard deviation is shown in Figure 6a. The average shows two peaks corresponding to the outer and inner leaflets of the bilayer, which are separated by ~50 Å. A low density region of ~70 Å width lies central to the bilayer region and is followed by three peaks of high density. The consistent features in the average density span ~270 Å from the outer leaflet of the bilayer to the innermost peak of density. There is no consistent density feature at lower radius; the center of the VLP has no radially organized density.

This cEM-derived density distribution differs from those derived from conventional EM techniques in reflecting the actual radial mass distribution, rather than the distribution of stain or contrasting medium. As a consequence, the observation that the peak corresponding to the inner bilayer is thicker than that corresponding to the outer bilayer indicates that more mass is present there. The standard deviation of the density distributions shows that the positions of the major peaks and of the trough are well defined in the particles. This analysis defines a density distribution that is common for particles of different radii, and hence defines the organization of the Gag protein, which is consistent with the broad range of VLP shapes and sizes. The Fourier–Bessel analysis verifies the consistency of these features, but the well-defined internal density, which is separated from the inner leaflet of the bilayer by a low density region, is easily visible in Figures 1, 2 and 4.

Discussion

The assembly of infectious retrovirus particles is based on the morphopoetic properties of the Gag protein. In all well

characterized retroviruses, this protein alone is capable of organizing the formation of virus-like particles that bud from the plasma membrane [1]. We explored this process using VLPs formed by expression of HIV-1 Gag in insect cells. These particles lack protease and a complete genome, so they are immature and non-infectious and hence a much more tractable system for structural studies than authentic HIV-1. The formation of VLPs must satisfy similar structural constraints to virus budding. Previous work had shown that the morphology of VLPs resembles that of the immature HIV-1 [5,8,14,15]. Our cEM observations of immature, paraformaldehyde-inactivated HIV-1 verified that the major features of the organization we describe for the VLP are shared by the authentic, immature virion.

The image of the VLP seen by cEM differs in several key points from the interpretations of previous work with stained specimens [8]. The cEM images show a much greater variability of particle size and reveal multi-sector structure of the particle. Quantification confirms that irregularity increases with particle size and suggests a consistent sector radius. These observations match the variation in size and shape observed with MLV by cEM [39]. and suggest it is a general feature of retroviruses.

Local order in the VLP

Exhaustive tests revealed no evidence of icosahedral symmetry in the VLPs or immature HIV-1 particles, but this does not mean that the particles lack organization. Local order was present at two levels. Firstly, freshly prepared VLPs were made up of 750 Å radius sectors. The submembrane Gag density is not homogeneous. Faults, or regions of lower density, separate facets along the particle circumference and at the sector interfaces. The VLPs lose this organization and become more spherical during storage at 4°C, suggesting that the local interactions of Gag proteins are more robust than those forming the sectors.

Secondly, the individual protein units packed into small crystalline patches with apparent p2 symmetry. These patches could be visualized within the VLPs, as well as after breakdown of the VLPs, to leave small crystalline areas. The organization of the Gag protein seen by cEM is a monoclinic (p2) arrangement of trimeric units with dimensions similar to the hexagonal one seen in previous work [8,40,41]. The unit cell angles within the plane of our p2 arrangement of trimers are close to those expected for a hexagonal lattice. The organization of this repeating unit bears a striking resemblance to that adopted by the fragments of SIV and HIV-1 MA in the crystals [42,43] in which a MA trimer is formed. Similarly, two-dimensional crystals of histidine-tagged MLV CA protein show an arrangement that can be indexed as either monoclinic (p2) or hexagonal (p6) [44]. The simplest interpretation of this repeating unit is a dimer of trimers in which the dimer interactions of CA [45–47] and the trimer ones of MA [42,43] are maintained. The departure from p6 symmetry could reflect stronger intra-dimer than inter-dimer interaction, or the tilt of the long Gag subunit in the curved particle.

Analysis of stereo images shows that the unit we have averaged represents internal density arising from the region that we ascribe to CA and NC. Side views of detergent-treated particles reveal a very rough surface near the position previously occupied by the membrane, indicating again that the strongest Gag–Gag interactions are away from the membrane, consistent with the importance of this region in budding [1,48]. The icosahedral nature of the virion was originally inferred from the interpretation of local patterns of protein positions and the angular form of the exterior of the mature particle [3,4,8,12,13,41]. Both could reflect the local ordering described here.

Radial arrangement of Gag domains

The arrangement of the Gag sequence in distinct domains is recapitulated in a radial density distribution that shows clear peaks (Figure 6a). The averaged radial density distributions showed a consistent distribution extending 270 Å from the edge of the outer leaflet of the bilayer to the innermost consistent feature. Density seen in cEM reflects mass rather than interaction with stain, indicating that these peaks must correspond to the polypeptide domains of Gag, which form the bulk of the internal density. Our knowledge of the three-dimensional structure of Gag is inferred from NMR and X-ray crystallographic structures of the mature viral proteins [21,22,42,43,49,50] . The cEM analysis provides the first glimpse of the overall three-dimensional structure of Gag, and a context for interpretation of the published structures in terms of the intact Gag molecule in the immature virion.

We assign the density immediately apposed to the inner surface of the membrane to MA, and the peaks at lower radius to CA and NC/P6. The assignment of density to MA is quite certain (Figure 6) and supported by the binding of HIV-1 Gag to lipids *in vitro* [51,52] and its cross linking to lipids in virions [53,54], as well as the requirement for myristylation [55,56] and positively-charged residues near the amino terminus [51,57] for MA function. The assignment of particular features to CA and NC/P6 is more tentative, as we cannot exclude the possibility that carboxy-terminal parts of the Gag protein are irregularly arranged and so lost in the average. The fact that the density assigned to CA is visualized as two partially separated peaks is consistent with the recently determined structure of purified HIV-1 CA [58], which suggests that CA is folded as two domains.

Our assignment of density features yields distances that differ from previous models that proposed a radial arrangement of 85 Å Gag 'rods' in which a compact MA domain was apposed to a folded CA domain [8]. This apposition is

inconsistent with the observation of an ~70 Å wide region of low density, which must correspond to protein that is not compactly folded. We hypothesize that this low density feature contains the carboxy-terminal third of MA and the amino-terminal residues of CA, and must have a different conformation than that seen in the high resolution structures of these domains. The MA sequences include a carboxy-terminal α helix in the crystal structure [42,43], which juts away from the putative membrane-binding portion and has been shown to affect the conformation of the amino-terminal portion of MA by *in vitro* membrane binding [52]. The CA sequences correspond to a β hairpin that buries the amino terminus of the CA protein, so that its amino group forms a salt bridge with D51 [45–47]. This CA region must rearrange upon cleavage.

The prediction that the sequences joining the compact regions of the MA and CA domains are extended draws support from comparative sequence analysis. In all retroviruses, except those of the lentivirus genus, one or more mature proteins are derived from the portion of Gag between MA and CA [2]. In all cases, these proteins are remarkably rich in proline and glycine, consistent with the possibility that this part of the Gag polypeptide is not folded. P12 of MLV is an example of such a protein, and indeed, the density features of immature MLV corresponding to those we assign to CA and NC are at lower radius than in HIV-1, and the gap correspondingly larger (~100 Å; E.M. Wilson-Kubalek and M. Yeager, personal communication). Furthermore, the observation that the deletion of the central 83 amino acids of MA does not abolish budding [59] argues against the requirement for the complete fold [49,50] for this process.

Mechanism of particle formation

Our results suggest a novel model for the Gag particle formation in which icosahedral symmetry plays no role. Particle formation begins with lateral interactions of Gag oligomers to form small ordered arrays, bound to the membrane through MA. Budding requires a further level of interaction which defines an angle between arrays. The most obvious candidate for this interaction is the RNA, which we have shown is present in all sizes of particle. Interaction with RNA would provide the foci for the formation of the semi-spherical sectors (Figure 6). In this view, RNA plays a central role in assembly by transforming the patches of locally interacting Gag proteins into a three-dimensionally ordered particle. Such a structural role for RNA has been demonstrated by *in vitro* reconstitution of particles from purified ASLV and HIV-1 Gag protein fragments [21,22]. Furthermore, the NC region, which interacts with RNA, contains one of the three essential 'assembly domains' that are required for retrovirus budding [1,48]. Separate nucleation by different RNAs, or different portions of the same RNA, would produce the multi-lobed structures that we observe in both the larger VLPs and authentic HIV-1. The occasional mature HIV-1 particles in which multiple cone-shaped capsids are observed (for example, Figure 10 of [4]) confirm that multiple copies of the genome can enter the authentic virion.

Conclusions

Cryo-electron microscopy of VLPs and immature HIV-1 has revealed the following features. First, both particles are heterogeneous in size and lack icosahedral symmetry. Second, both particles comprise sectors of defined (750 Å) radius separated by faults. This organization is labile and lost upon incubation at 4°C, which renders the particles spherical. Third, Gag proteins interact locally to generate small (p2) arrays that form facets within the sectors and appear to contain a dimer of trimers repeating unit. Fourth, particles share a common radial density profile, in which the arrangement of features recapitulates the polypeptide domain organization of Gag, although certain features of the high-resolution structures of isolated Gag domains must be modified to match the observed density for the intact Gag molecule *in situ*. In particular, the carboxy-terminal region of MA and the amino-terminal regions of CA form an extended structure of 70 Å length.

We propose a mechanism for virion formation in which local interactions between Gag proteins yields arrays that are organized into sectors for budding by the interaction with RNA. The ability of this assembly mechanism to tolerate varying lengths of RNA is consistent with the ease of incorporating extra sequences into retroviral genomes. This model would predict that particles with larger amounts of nucleic acid would have a larger number of lobes and be more irregular rather than simply display a larger diameter. The fact that Gag of HIV-1 shares polypeptide domain structure with other retroviruses [2,48] and cEM of MLV suggest that the mechanism may be a general one.

This first cEM study of the HIV-1 Gag particle raises a wealth of immediate questions. Among them are the structural effects of mutations that affect particle formation, alterations in RNA length and the cleavages that lead to maturation. The ability to generate particles in defined systems such as used here for the VLPs will allow these questions to be addressed systematically. The methodology opens the way for providing a context for the high-resolution structures of HIV-1 Gag domains that are becoming available. Our structural model provides a basis for exploring the mechanism of retrovirus assembly in greater detail.

Materials and methods

Particle preparation

HIV-1 VLPs were prepared using the recombinant baculovirus AcNPV-gag12myr in *Spodoptera fugiperda* cells as described previously [14,15,36].

Preparation of authentic immature HIV-1 particles

HIV-1 particles were produced by infection of MT4 cells [36] with an infectious proviral clone, pNL4-3, for 24 h in the presence of protease

inhibitor RO31-8959 [60] to block their maturation and concentrated as described [36]. Pellets were resuspended in ice cold PBS containing 2.5% paraformaldehyde and allowed to stand for 30 min on ice before processing for cEM.

Microscopy and image processing

Cryo-electron microscopy was performed as described previously using either a Philips EM400 microscope operated at 80 kV or a Philips CM200FEG operated at 200 kV [34]. Tests for icosahedral symmetry were performed by exhaustive runs of the programs EMICOFV, EMICOORG, SIMPLEX and EMPFTREF1 [30,34] using a variety of resolution ranges and radial masks. A more complete description of the programs and their use can be found at http://www.EMBL-Heidelberg.DE/ExternalInfo/fuller/EMBL_Virus_Structure.html.

Analysis of crystalline patches was performed using the SEMPER 6 image processing package (Synoptics, Cambridge, UK). The analysis used a motif generated by averaging positions of high autocorrelation in a high pass, low pass filtered image. Symmetry (p2, p3 or p6) was imposed upon the motif by real space averaging before use in alignment to test the presence of this symmetry in the motif.

The calculation of the radial density distribution was performed using a Fourier–Bessel expansion method. The center of the particle was defined by cross correlation and the radial variation in density from the center was extracted for each angle between 0 and 2 π in one degree steps. These radial densities were padded, Fourier transformed and the Fourier–Bessel expansion calculated at each root of $J_n(2\pi rR)$ [39] by integration using a 10 point formula within the particle radius. The coefficient of each term is proportional to the three-dimensional density at that point. The profiles from individual particles were averaged by aligning the density corresponding to the two leaflets of the bilayer. The program for performing the averaging is written in FORTRAN using standard subroutines [61] and is available upon request. Tests of the implementation included its use on projections of Semliki Forest virus [34] and the enveloped bacteriophage PRD1 [62] .

Immunocytochemistry

The presence of nucleic acid in the VLPs was tested by using an anti-RNA antibody (D444) [23–25] and a modification of our post-sectioning fixation technique [63] on freeze-substituted samples. Controls for the specificity of labeling included the positive stranded RNA Semliki Forest virus and the DNA virus, Adenovirus 2, and were stained in parallel to the VLP sample.

Acknowledgements

The authors are pleased to acknowledge our colleagues at the European Molecular Biology Laboratory for helpful discussions and encouragement during the course of this work, Eric Barklis (OHSU, Portland) for useful discussions and comments on the work, Milan Nermut (NIBSC, London) for imparting his enthusiasm for the problem of retrovirus assembly and for helpful criticism of the results, Pierre Boulanger (INSERM, Montpellier) for providing the baculovirus clones used in the work and for his encouragement and useful discussion, Dan Eilat (Hadasah University Hospital, Jerusalem) for providing the anti-RNA ascites, D444, used in the immunocytochemistry, Christina Ochsenbauer (ATV DKFZ, Heidelberg) for the preparation of the immature HIV-1 particles, Valerie Bosch (ATV DKFZ, Heidelberg) for the use of her laboratory's P3 facilities, Mark Yeager and Elizabeth Wilson-Kubalek (Scripps Research Institute) for discussing their work prior to its publication, so that the similarity between the HIV-1 and MLV systems became clear.

References

1. Wills JW, Craven RC: **Form, function, and use of retroviral Gag proteins.** *AIDS* 1991, **5:**639-654.
2. Leis J, Baltimore D, Bishop JM, Coffin J, Fleissner E, Goff SP, *et al.*: **Standardized and simplified nomenclature for proteins common to all retroviruses.** *J Virol* 1988, **62:**1808-1809.
3. Gelderblom HR, Hausmann EHS, Özrel M, Pauli G, Koch MA: **Fine structure of human immunodeficiency virus (HIV) and immunolocalization of structural proteins.** *Virology* 1987, **156:**171-176.
4. Gelderblom HR: **Assembly and morphology of HIV: potential effect of structure on viral function.** *AIDS* 1991, **5:**617-638.
5. Gheysen D, Jacobs E, de Foresta F, Thiriart C, Francotte M, Thinnes D, *et al.*: **Assembly and release of HIV-1 precursor Pr55gag virus-like particles from recombinant baculovirus-infected insect cells.** *Cell* 1989, **59:**103-112.
6. Ashorn B, McQuade JM, Thaisvivongs S, Tomasselli AG, Tarpley WG, Moss B: **An inhibitor of the protease blocks maturation of human and simian immunodeficiency virus and the spread of infection.** *Proc Natl Acad Sci USA* 1990, **87:**7472-7476.
7. Stewart L, Schatz G, Vogt VM: **Properties of avian retrovirus particles defective in viral protease.** *J Virol* 1990, **64:**5076-5092.
8. Nermut MV, Hockley DJ, Jowett JBM, Jones IM, Garreau M, Thomas D: **Fullerene-like organization of the HIV gag-protein shell in virus like particles produced by recombinant baculovirus.** *Virology* 1994, **198:**288-296.
9. Nermut MV, Frank H, Schäfer W: **Properties of mouse leukemia viruses: III Electron microscopic appearance as revealed after conventional preparation techniques as well as freeze drying and freeze etching.** *Virology* 1972, **49:**345-358.
10. Sarkar NH, Moore DH: **Surface structure of mouse mammary tumor virus.** *Virology* 1974, **61:**38-55.
11. Yoshinaka Y, Luftig RB: **Murine leukemia virus morphogenesis: cleavage of P70 can be accompanied by a shift from a concentrically coiled internal strand ("immature") to collapsed ("mature") form of the virus core.** *Proc Natl Acad Sci USA* 1977, **74:**3446-3450.
12. Marx PA, Munn RJ, Joy KI: **Computer emulation of thin section electron microscopy predicts an envelope associated icosadeltahedral capsid for human immunodeficiency virus.** *Lab Invest* 1988, **58:**112-118.
13. Höglund S, Öfverstedt LG, Nilson A, Lundqvist P, Gelderbloom HR, Ozel M, *et al.*: **Spatial visualization of the maturing HIV-1 core and its linkage to the envelope.** *AIDS Res Hum Retroviruses* 1992, **8:**1-7.
14. Royer M, Cerutti M, Gray B, Hong S-S, Devauchelle G, Boulanger P: **Functional domain of HIV-1 gag polyprotein expressed in baculovirus infected cells.** *Virology* 1991, **184:**417-422.
15. Royer M, Hong S-S, Gay B, Cerutti M, Boulanger P: **Expression and extracellular release of human immunodeficiency virus type 1 Gag precursors by recombinant baculovirus-infected cells.** *J Virol* 1992, **66:**3230-3235.
16. Delchambre M, Gheysen D, Thines D, Thiriart C, Jacobs E, Vedin E, *et al.*: **The GAG precursor of simian immunodeficiency virus assembles into virus like particles.** *EMBO J* 1989, **8:**2653-2660.
17. Hockley DJ, Wood RD, Jacobs JP, Garrett AJ: **Electron microscopy of human immunodeficiency virus.** *J Gen Virol* 1988, **69:**2455-2469.
18. Vernon SK, Murthy S, Wilhelm J, Chanda PK, Kalyan N, Lee S-G, *et al.*: **Ultrastructural characterization of human immunodeficiency virus type 1 Gag containing particles assembled in a recombinant adenovirus vector system.** *J Gen Virol* 1991, **72:**1243-1251.
19. Wagner R, Fliessbach H, Wanner G, Motz M, Niedrig M, Deby G, *et al.*: **Immunological reactivity of a human immunodeficiency virus type I derived peptide representing a consensus sequence of the GP120 major neutralizing region V3.** *Arch Virol* 1992, **127:**117-137.
20. Fuller SD: **The T = 4 envelope of sindbis virus is organized by complementary interactions with a T = 3 icosahedral capsid.** *Cell* 1987, **48:**923-934.
21. Campbell SJ, Vogt VM: **Self-assembly *in vitro* of purified CA-NC proteins from Rous sarcoma virus and human immunodeficiency virus type 1.** *J Virol* 1995, **69:**6487-6497.
22. Campbell S, Vogt VM: ***In vitro* assembly of virus-like particles with Rous sarcoma virus Gag deletion mutants: identification of the p10 domain as a morphological determinal in the formation of spherical particles.** *J Virol* 1997, **71:**4425-4435.
23. Reines D: **RNA polymerase II elongation complex. Elongation complexes purified using an anti-RNA anitbody do not contain initiation factor alpha.** *J Biol Chem* 1991, **266:**10510-10517.
24. Reines D: **Purification of RNA using an anti-RNA antibody.** *Anal Biochem* 1991, **192:**367-372.
25. Thiry M, Puvion-Dutilleul: **Differential distribution of single-stranded DNA, double stranded DNA and RNA in Adenovirus-induced intranuclear region of HeLa Cells.** *J Histochem Cytochem* 1993, **43:**749-759.
26. Conway JF, Cheng N, Zlotnick A, Wingfield PT, Stahl SJ, Steven AC: **Visualization of the 4-helix bundle in the hepatitis B virus capsid by cryo-electron microscopy.** *Nature* 1997, **386:**91-94.

27. Böttcher B, Wynne SA, Crowther RA: **Determination of the fold of the core protein of hepatitis B virus by electron cryomicroscopy.** *Nature* 1997, **386:**88-91.
28. Crowther R, Kiselev NA, Böttcher B, Berriman JA, Borisova GP, Ose V, *et al.*: **Three-dimensional structure of hepatitis B virus core particles determined by electron cryo-microscopy.** *Cell* 1994, **77:**943-950.
29. Kenney J: **Evolutionary conservation in the hepatitis B core: comparison of human and duck cores.** *Structure* 1995, **3:**1009-1020.
30. Fuller SD, Butcher SJ, Cheng RH, Baker TS: **Three-dimensional reconstruction of icosahedral particles: the uncommon line.** *J Struct Biol* 1996, **116:**48-65.
31. Crowther RA, Amos LA, Finch JT, De Rosier DJ, Klug A: **Three-dimensional reconstructions of spherical viruses by Fourier synthesis from electron micrographs.** *Nature* 1970, **226:**421-423.
32. Crowther RA, Amos LA: **Three-dimensional image reconstruction of some small spherical viruses.** *Cold Spring Harb Symp Quant Biol* 1972, **36:**489-494.
33. Cheng RH, Kuhn RJ, Olson NH, Rossmann MG, Choi H-K, Smith TJ, *et al.*: **Nucleocapsid and glycoprotein organization in an enveloped virus.** *Cell* 1995, **80:**621-630.
34. Fuller SD, Berriman JA, Butcher SJ, Gowen BE: **Low pH induces the swivelling of the glycoprotein heterodimers in the Semliki Forest virus spike complex.** *Cell* 1995, **81:**715-725.
35. Paredes AM, Brown DT, Rothnagel R, Chiu W, Schoepp RJ, Johnston RE, *et al.*: **Three-dimensional structure of a membrane-containing virus.** *Proc Nat Acad Sci USA* 1993, **90:**9095-9099.
36. Wilk T, Pfeiffer T, Bukovsky A, Moldenhauer G, Bosch V: **Glycoprotein incorporation and HIV-1 infectivity despite exchange of the gp160 membrane-spanning domain.** *Virology* 1996, **218:**269-274.
37. Holser WT: **Two-dimensional crystal groups.** *Z Kristallogr Kristallgeom Kristallphys Kristallchem* 1958, **110:**266-281.
38. van Heel M: **Similarity measures between images.** *Ultramicroscopy* 1987, **21:**95-100.
39. Jackson JD: *Classical Electrodynamics.* New York: John Wiley and Sons, Inc.; 1962.
40. Zhang WH, Hockley D, Nermut MV, Morikawa Y, Jones IA: **Gag–Gag interactions in the C-terminal domain of human immunodeficiency virus type 1 p24 capsid antigen are essential for Gag particle assembly.** *J Gen Virol* 1996, **77:**743-751.
41. Nermut MV, Grief C, Hashmi S, Hockley DJ: **Further evidence of icosahedral symmetry in human and simian immunodeficiency virus.** *AIDS Res Hum Retroviruses* 1993, **9:**929-938.
42. Rao Z, Belyaev AS, Fry E, Jones IM, Stuart DI: **Crystal structure of the SIV matrix antigen and implications for virus assembly.** *Nature* 1995, **378:**743-747.
43. Hill CP, Worthylake D, Bancroft DP, Christensen AM, Sundquist WI: **Crystal structures of the trimeric human immunodeficiency virus type 1 matrix protein: implications for membrane association and assembly.** *Proc Natl Acad Sci USA* 1996, **93:**3099-3104.
44. Barklis E, J M, Wilkens S, Schabtach E, Schmid M, Fuller S, *et al.*: **Structural analysis of membrane bound retrovirus capsid proteins.** *EMBO J* 1996, **16:**1199-1213.
45. Gitti RK, Lee BM, Walker J, Summers MF, Yoo S, Sundquist WI: **Structure of the amino-terminal core domain of the HIV-1 capsid protein.** *Science* 1996, **273:**231-235.
46. Gamble TR, Vajdos F, Yoo S, Worthylake DK, Houseweart J, Sundquist WI: **Crystal structure of human cyclophilin A bound to the amino terminal domain of HIV-1 capsid.** *Cell* 1996, **87:**1285-1294.
47. Momany C, Kovari LC, Prongay AJ, Keller W, Gitti RK, Lee BM, *et al.*: **Crystal structure of dimeric HIV-1 capsid protein.** *Nature Struct Biol* 1996, **3:**763-770.
48. Parent LJ, Bennett RP, Craven RC, Nelle TD, Krishna NK, Bowzard JB, *et al.*: **Positionally independent and exchangeable late budding functions of the Rous sarcoma virus and human immunodeficiency virus Gag proteins.** *J Virol* 1995, **70:**5455-5460.
49. Massiah MA, Starich MR, Paschal C, Summers MF, Christensen AM, Sundquist WI: **Three-dimensional structure of the human immunodeficiency virus type 1 matrix protein.** *J Mol Biol* 1994, **244:**198-223.
50. Matthews S, Barlow P, Boyd J, Barton G, Russell R, Mills H, *et al.*: **Structural similarity between the p17 matrix protein of HIV and interferon-gamma.** *Nature* 1994, **370:**666-668.
51. Zhou K, Parent LJ, Wills JW, Resh MD: **Identification of a membrane binding domain within the amino-terminal region of human immunodeficiency virus type 1 Gag protein which interacts with acidic phospholipids.** *J Virol* 1994, **68:**2556-2569.
52. Zhou W, Resh MD: **Differential membrane binding of the human immunodeficiency virus type 1 matrix protein.** *J Virol* 1996, **70:**8540-8548.
53. Pepinsky RB: **Localization of lipid–protein and protein–protein interaction within the murine retrovirus gag precursor by a novel peptide mapping technique.** *J Biol Chem* 1983, **258:**11229-11235.
54. Pepinsky RB, Vogt VM: **Fine structure analyses of lipid–protein and protein–protein interactions of *gag* protein p19 of the avian sarcoma and leukemia viruses by cyanogen bromide mapping.** *J Virol* 1984, **52:**145-153.
55. Bryant M, Ratner L: **Myristoylation-dependant replication and assembly of human immunodeficiency virus 1.** *Proc Natl Acad Sci USA* 1990, **87:**523-527.
56. Göttlinger HG, Sodroski JG, Hasaltine WA: **Role of capsid precursor processing and myristylation in morphogenesis and infectivity of human immunodeficiency virus type 1.** *Proc Natl Acad Sci USA* 1989, **86:**5781-5785.
57. Freed EO, Martin MA: **Domains of the human immunodeficiency virus type 1 matrix protein and gp41 cytoplasmic tail required for envelope incorporation into virions.** *J Virol* 1996, **70:**341-351.
58. Gamble TR, Yoo S, Vajdos F, Von Schwedler UK, McCutcheon J, Sundquist WI: **Structure of the carboxy-terminal dimerization domain of HIV-1 capsid protein.** *Science* 1997, in press.
59. Fäcke M, Janetzko A, Shoeman RL, Kräusslich H-G: **A large deletion in the matrix domain of the human inmmunodeficiency virus gag gene redirects virus particle assembly from the plasma membrane to the endoplasmic reticulum.** *J Virol* 1993, **67:**4972-4980.
60. Roberts NA, Martin JA, Kinchington D, Broadhurst AV, Craig JC, Duncan IS, *et al.*: **Rational design of peptide-based HIV protease inhibitors.** *Science* 1990, **248:**358-361.
61. Press WH, Teukolsky SA, Vetterling WT, Flannnery BP: *Numerical Recipes in Fortran: The Art of Scientific Computing.* Cambridge: Cambridge University Press; 1992.
62. Butcher SJ, Bamford DH, Fuller SD: **DNA packaging orders the membrane of bacteriophage PRD1.** *EMBO J* 1995, **14:**6078-6086.
63. Gowen BE, Buendia B, Karsenti E, Fuller SD: **Post-embedding α-tubulin immunolabelling of isolated centrosomes.** *Histochem J* 1995, **27:**240-246.

Because *Current Biology* operates a 'Continuous Publication System' for Research Papers, this paper has been published on the internet before being printed. The paper can be accessed from http://biomednet.com/cbiology/cub – for further information, see the explanation on the contents page.